Generalized dimensions for fluctuations in the solar wind

Wiesław M. Macek*

*Faculty of Mathematics and Natural Sciences. College of Sciences, Cardinal Stefan Wyszyński University,
Dewajtis 5, 01-815 Warsaw, Poland
and Space Research Centre, Polish Academy of Sciences, Bartycka 18 A, 00-716 Warsaw, Poland*

Roberto Bruno and Giuseppe Consolini

Istituto di Fisica dello Spazio Interplanetario, Istituto Nazionale di Astrofisica, Via Fosso del Cavaliere 100, 00-133 Roma, Italy

We analyze time series of velocities of the solar wind plasma including the outward-directed component of Alfvénic turbulence within slow wind observed by the Helios 2 spacecraft in the inner heliosphere. We demonstrate that the influence of noise in the data can be efficiently reduced by a singular-value decomposition filter. The resulting generalized dimensions show a multifractal structure of the solar wind attractor in the inner heliosphere. The obtained multifractal spectrum is consistent with that for the multifractal measure on the self-similar weighted baker's map with two parameters describing uniform compression and natural invariant measure on the attractor of the system.

The generalized dimensions of attractors are important characteristics of *complex* dynamical systems [1]. Since these dimensions are related to frequencies with which typical orbits in phase space visit different regions of the attractors, they provide information about dynamics of the systems [2]. If the measure has different fractal dimensions on different parts of the support, the measure is multifractal [3].

The question of multifractality is of great importance also for the solar wind community, because it allows us to investigate the nature of interplanetary hydromagnetic turbulence, e.g., [4–6]. Therefore, following these applications, we consider the inner heliosphere. The solar wind plasma flowing supersonically outward from the Sun is quite well modeled within the framework of the hydromagnetic theory. This continuous flow has two forms: slow ($\approx$400 km s^{-1}) and fast ($\approx$700 km s^{-1}) [7]. We limit our study to the low-speed stream. Indication for a chaotic attractor in the slow solar wind has been given in [8–10]. In particular, Macek [8] has calculated the correlation dimension of the reconstructed attractor. Further, Macek and Redaelli [9] have shown that the Kolmogorov entropy of the attractor is *positive* and finite, as it holds for a *chaotic* system. The entropy is plausibly constrained by a *positive* local Lyapunov exponent that would exhibit sensitive dependence on initial conditions of the system.

We have extended our previous results on the dimensional time series analysis [8]. Namely, we have applied the technique that allows a realistic calculation of the generalized dimensions of the solar wind flow directly from the cleaned experimental signal by using the Grassberger and Procaccia method [11]. The resulting spectrum of dimensions shows the multifractal structure of the solar wind in the inner heliosphere [10]. In this paper we demonstrate the influence of

noise on these results and show that noise can efficiently be reduced by a singular-value decomposition filter. The obtained multifractal spectrum of the solar wind attractor reconstructed in the phase space is consistent with that for the multifractal measure on the self-similar weighted baker's map.

We analyze the Helios 2 data using plasma parameters measured *in situ* in the inner heliosphere [7]. The X-velocity (mainly radial) component of the plasma flow, v, has been investigated in [8,9]. However, it is known that various disturbances are superimposed on the overall structure of the solar wind, including mainly Alfvén waves. Therefore, in this paper we take also into account Alfvénic fluctuations of the flow. Namely, in this paper we analyze the radial $(X-)$ component of one of the Elsässer variables, $x = z_+$, representing Alfvénic fluctuations propagating outward from the Sun. We have $z_+ = v + v_A$ for the unperturbed magnetic field B_o pointing to the Sun and $z_+ = v - v_A$ for B_o pointing away from the Sun, where $v_A = B/(\mu_o \rho)^{1/2}$ is the Alfvénic velocity calculated from the experimental data: the radial component of the magnetic field of the plasma B and the mass density ρ (μ_o is the permeability of free space). Assuming absence of radial evolution, we have merged two selected time intervals separated by about 0.5 AU as observed by the Helios 2 spacecraft in 1977 (i) from 116:00 to 121:21 (day:hour) at distances 0.30–0.34 AU and (ii) from 348:00 to 357:00 at 0.82–0.88 AU from the Sun. These raw data of v and v_A, $N = 26,163$ points, with sampling time of $\Delta t = 40.5$ s, are shown in Fig. 1(a). Small gaps ($\leq 3 \Delta t$) have been interpolated linearly, but larger gaps have been removed from the data sets.

As in [10], slow trends (i) $344.596 - 20.291\,t - 0.358\,t^2$ and $88.608 - 452.349\,t + 343.471\,t^2$ and (ii) $397.847 - 291.602\,t - 241.999\,t^2$ and $-30.050 + 87.756\,t - 77.773\,t^2$ (with t being a fraction of a given sample) were subtracted from the original data $v(t_i)$ and $v_A(t_i)$, correspondingly, where these values are given in km s^{-1}, and $i = 1, \ldots, N$. The

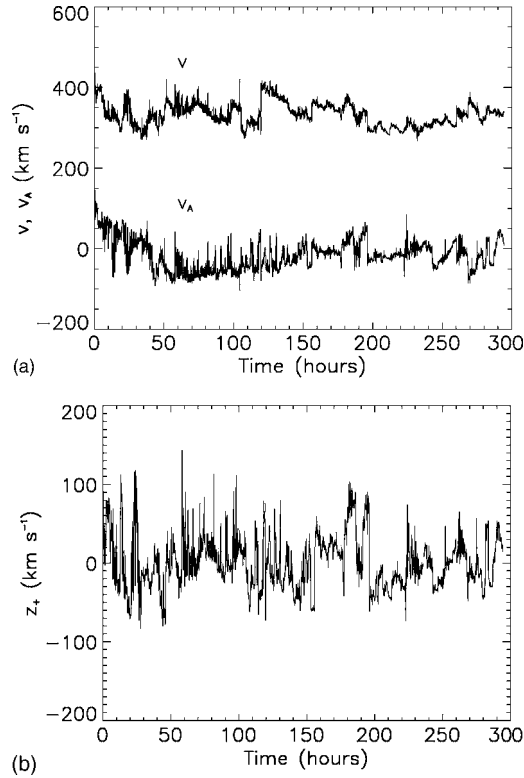*Email address: macek@cbk.waw.pl; http://www.cbk.waw.pl/ ~macek

FIG. 1. (a) The raw data of the radial flow velocity with Alfvénic velocity, v and v_A, observed by the Helios 2 spacecraft in 1977 from 116:00 to 121:21 (day:hour) at distance 0.3 AU and from 348:00 to 357:00 at distance 0.9 AU from the Sun. (b) The Elsässer variable $z_+ = v \pm v_A$ for B_o pointing to/away from the Sun for the detrended and filtered data using singular-value decomposition with the five largest eigenvalues.

data with the initial several-percent noise level were (eight-fold) smoothed (replacing each data point with the average of itself and its two nearest neighbors). Next, the data have been filtered using a method of singular-value decomposition analysis described by Albano *et al.* [12]. As argued in Ref. [8] we use five principal eigenvalues. The detrended and filtered data for the radial component of the Elsässer variable $x = z_+$ are shown in Fig. 1(b).

Table I summarizes selected calculated characteristics of the detrended data cleaned by using the singular-value decomposition filter; see also Ref. [10]. The probability distributions are clearly non-Gaussian. We have a large skewness of ~ 0.59 (as compared with its normal standard deviation 0.02) and a large kurtosis of 0.37 (the latter was small for the

TABLE I. Characteristics of the solar wind filtered data, z_+.

Skewness, κ_3	0.59
Kurtosis, κ_4	0.37
Relative complexity	0.09
Autocorrelation time, t_a	7.05×10^3 s
Capacity dimension, D_0	3.9
Correlation dimension, D_2[a]	3.4

[a]The average slope for $6 \leq m \leq 10$ is taken as $(q-1)D_q$.

analysis with no magnetic field); see Ref. [8]. We have also estimated the Lempel-Ziv measure of *complexity*, relative to white noise [13]. The calculated value ~ 0.09 is even smaller than in [8] (≈ 0.20); maximal complexity, or randomness, would have a value of 1.0, while a value of zero denotes perfect deterministic nonlinear predictability.

We choose a time delay $\tau = 174 \, \Delta t$, equal to the autocorrelation time t_a where the autocorrelation function decreases to $1/e$, $[\langle x(t)x(t+t_a)\rangle - \langle x(t)\rangle^2]/\sigma^2 = 1/e$, with average velocity $\langle x \rangle = 0.622$ km s^{-1} and standard deviation $\sigma = 33.514$ km s^{-1}; see Table I. This makes certain that $x(t)$ and $x(t+\tau)$ are at least linearly time independent, e.g., Ref. [2]. Using our time series of equally spaced, detrended, and cleaned data, we construct a large number of vectors $\mathbf{X}(t_i) = \{x(t_i), x(t_i+\tau), \ldots, x[t_i+(m-1)\tau]\}$ in the embedding phase space of dimension m, where $i = 1, \ldots, n$ with $n = N - (m-1)\tau$. Then, we divide this space into a large number $M(r)$ of equal hypercubes of size r which cover the presumed attractor. If p_j is the probability measure that a point from a time series falls in a typical jth hypercube, using the q-order function $I_q(r) = \Sigma(p_j)^q$, $j = 1, \ldots, M$, the q-order generalized dimension is given by [2]

$$D_q = \frac{1}{q-1} \lim_{r \to 0} \frac{\ln I_q(r)}{\ln r}. \tag{1}$$

We see from Eq. (1) that the larger q is, the more strongly are the higher-probability cubes (visited more frequently by a trajectory) weighted in the sum for $I_q(r)$. Only if $q=0$, all the cubes are counted equally, $I_0 = M$, and we recover the box-counting dimension, D_0.

Writing $I_q(r) = \Sigma p_j(p_j)^{q-1}$ as a weighted average $\langle (p_j)^{q-1} \rangle$, one can associate bulk with the generalized average probability per hypercube $\mu = \sqrt[q-1]{\langle (p_j)^{q-1} \rangle}$, and identify D_q as a scaling of bulk with size, $\mu \propto r^{D_q}$. Since the data cannot constrain well the capacity dimension D_0, we look for higher-order dimensions, which quantify the multifractality of the probability measure on the attractor. For example, the limit $q \to 1$ leads to a geometrical average (the information dimension). For $q=2$ the generalized average is the ordinary arithmetic average (the standard correlation dimension), and for $q=3$ it is a root-mean-square average. In practice, for a given m and r,

$$p_j \simeq \frac{1}{n - 2n_c - 1} \sum_{i=n_c+1}^{n} \theta(r - |\mathbf{X}(t_i) - \mathbf{X}(t_j)|) \tag{2}$$

with $\theta(x)$ being the unit step function, and $n_c = 4$ is the Theiler's correction [14]. Finally, $I_q(r)$ is taken to be equal to the generalized q-point correlation sum [11]

$$C_q(m,r) = \frac{1}{n_{\text{ref}}} \sum_{j=1}^{n_{\text{ref}}} (p_j)^{q-1}, \tag{3}$$

where $n_{\text{ref}} = 5000$ is the number of reference vectors. For large dimensions m and small distances r in the scaling region it can be argued that $C_q(m,r) \propto r^{(q-1)D_q}$, where D_q is an approximation of the ideal limit $r \to 0$ in Eq. (1) for a given q [11].
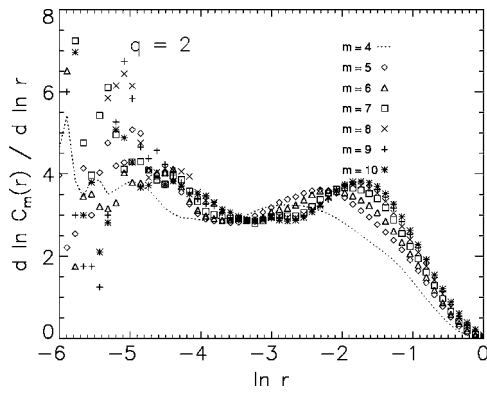
FIG. 2. The slopes $D_{2,m}(r)=d[\ln C_m(r)]/d(\ln r)$ of the correlation sum $C_m(r)$ versus $\ln r$ (normalized) obtained for detrended and filtered data are shown for various embedding dimensions m.

First, we calculate the natural logarithm of the standard ($q=2$) correlation sum $C_m(r)=C_2(m,r)$ versus $\ln r$ (normalized) for various embedding dimensions: $m=4$ (dotted curve), $m=5$ (diamonds), $m=6$ (triangles), $m=7$ (squares), $m=8$ (crosses), $m=9$ (pluses), and $m=10$ (stars). The slopes $D_{2,m}(r)=\mathrm{d}[\ln C_m(r)]/d(\ln r)$ in the scaling region of r should provide the correlated dimension. The results obtained using the moving average filter and singular-value decomposition linear filter are presented in Fig. 2, while those obtained using the nonlinear Schreiber filters have been discussed in [8,9]. Since the correlation sum is simply an arithmetic average over the numbers of neighbors, this can yield meaningful results for the dimension even when the number of neighbors available for some reference points is limited in most real dynamical systems. If the D-dimensional attractor exists, we expect a plateau of the slopes for $m \geq D$ and in the worst case for $m>2D$. For m large enough an average slope in the scaling region indicates a proper correlation dimension D_2. We have a clear plateau which appears already for $m=4$ (dotted curve) and $m=5$. For higher dimensions, $m \geq 8$, the plateau is still present but more smeared out by the statistical fluctuations at small r. In our case of the singular-value decomposition filter the slope of the calculated correlation sum saturates for $m>5$, with an average for $6 \leq m \leq 10$ of $D_2=3.35\pm0.21$; see Ref. [8]. This is consistent with the attractor of the low-dimension.

Second, the generalized dimensions D_q in Eq. (1) as a function of q are shown in Fig. 3. It is well known that for $q<0$ we have some basic statistical problems. Nevertheless, in spite of large statistical errors (especially for $q<0$) the multifractal character of the measure can still be discerned. Therefore, one can say that the spectrum of dimensions still exhibits the multifractal structure of the slow solar wind in the inner heliosphere. In order to quantify that multifractality we use a simple two-dimensional analytical model of the dynamical system. Namely, we consider the generalized self-similar baker's map acting on the unit square with two parameters describing uniform compression and natural invariant measure on the attractor of the system [2]. In this model, the probability of visiting one region of the square is p (say $p \leq 1/2$), so that the probability of visiting the remaining region is $1-p$. Another parameter $s \leq 1/2$ describes both the
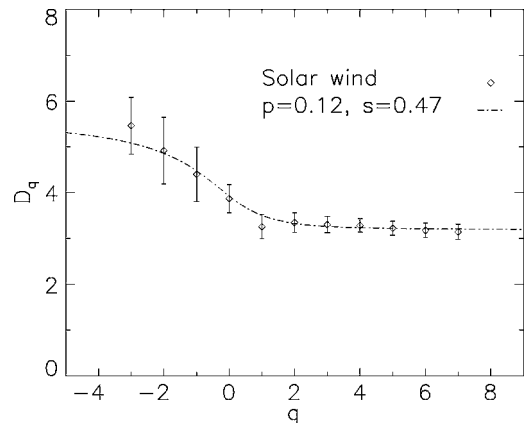

FIG. 3. The generalized dimensions D_q in Eq. (1) as a function of q. The correlation dimension is $D_2=3.4\pm0.2$ (see Table I). The values of D_q+3 are calculated analytically for the weighted baker's map with $p=0.12$ and $s=0.47$ (dashed-dotted).

uniform stretching and folding in the phase space, i.e., s is a folding and dissipation parameter.

In the case of uniform compression the results can be obtained analytically; for any q in Eq. (1) one has for the generalized dimension of the attractor projected onto one axis [2]

$$(q-1)D_q = \frac{\ln[p^q+(1-p)^q]}{\ln s}. \tag{4}$$

In the absence of dissipation ($s=1/2$) one recovers the formula for the well-known multifractal cascade p model for fully developed turbulence [15], which obviously corresponds to the generalized weighted Cantor set [1]. In particular, the usual middle one-third Cantor set without any multifractality is recovered with $p=1/2$ and $s=1/3$. The difference of the maximum and minimum dimensions, associated with the least-dense and most-dense points on the attractor, correspondingly, is $D_{-\infty}-D_{+\infty}=\ln(1/p-1)/\ln(1/s)$ and in the limit $p \rightarrow 0$ this difference rises to infinity. Hence, for a given s the parameter p can be regarded as a degree of multifractality. For illustration the results of D_q+3 fitted to the experimental values with $p=0.12$ and $s=0.47$ in Eq. (4) are also shown in Fig. 3 by a dashed-dotted line. We see that the multifractal spectrum of the solar wind is roughly consistent with that for the multifractal measure on the self-similar weighted baker's map. The action of this map exhibits stretching and folding properties leading to sensitive dependence on initial conditions; it could be a suitable model for a solar wind behavior. Clearly, the obtained values of the parameters s and p demonstrate small dissipation of the complex solar wind system and show that some cubes that cover the attractor of our dynamical system are visited one order of magnitude more frequently than some other cubes, as is illustrated in our previous paper, see Fig. 5 of Ref. [8].

The obtained measures of the attractor have been subjected to the surrogate data test [16]. As has been demonstrated in Fig. 8 of Ref. [8], if the original data are indeed deterministic, analysis of these surrogate data will provide values that are statistically distinct from those derived for the

original data. In particular, the slope of the correlation sum increases with m (no saturation), and Lempel-Ziv complexity calculated for shuffled data becomes clearly 1.0, as it should be for a purely stochastic system. Again, we have found that the solar wind data are sensitive to this test.

In conclusion, we have shown that the singular-value decomposition filter removes some amount of noise, which is sufficient to calculate the generalized dimensions of the solar wind attractor reconstructed in the phase space. The obtained multifractal spectrum of this attractor is consistent with that for the multifractal measure on the self-similar weighted baker's map. The action of this map exhibits stretching and folding properties leading to sensitive dependence on initial conditions. The values of the parameters fitted demonstrate small dissipation of the complex solar wind dynamical system and show that some cubes that cover the attractor in phase space are visited at least one order of magnitude more frequently than other cubes. The obtained characteristics of the attractor are significantly different from those of the surrogate data. Thus these results show multifractal structure of the solar wind in the inner heliosphere. Hence we suggest that there exists an inertial manifold for the solar wind, in which the system has *multifractal* structure, and where noise is certainly not dominant. The multifractal structure, convected by the wind, might probably be related to the complex topology shown by the magnetic field at the source regions of the solar wind.

[1] H. G. E. Hentschel and I. Procaccia, Physica D **8**, 435 (1983); P. Grassberger, Phys. Lett. **97A**, 227 (1983); T. C. Halsey, M. H. Jensen, L. P. Kadanoff, I. Procaccia, and B. I. Shraiman, Phys. Rev. A **33**, 1141 (1986).

[2] E. Ott, *Chaos in Dynamical Systems* (Cambridge University Press, Cambridge, 1993).

[3] B. B. Mandelbrot, Pure Appl. Geophys. **131**, 5 (1989).

[4] L. F. Burlaga, Geophys. Res. Lett. **18**, 69 (1991).

[5] E. Marsch, C.-Y. Tu, and H. Rosenbauer, Ann. Geophys. **14**, 259 (1996).

[6] R. Bruno, V. Carbone, P. Veltri, E. Pietropaolo, and B. Bavassano, Planet. Space Sci. **49**, 1201 (2001).

[7] R. Schwenn, in *Physics of the Inner Heliosphere*, edited by R. Schwenn and E. Marsch (Springer-Verlag, Berlin, 1990), Vol. 20, pp. 99–182.

[8] W. M. Macek, Physica D **122**, 254 (1998).

[9] W. M. Macek and S. Redaelli, Phys. Rev. E **62**, 6496 (2000).

[10] W. M. Macek, in *Experimental Chaos*, edited by S. Boccaletti, B. J. Gluckman, J. Kurths, L. M. Pecora, and M. L. Spano, AIP Conf. Proc. No. 622 (American Institute of Physics, Melville, NY, 2002), pp. 74–79.

[11] P. Grassberger and I. Procaccia, Physica D **9**, 189 (1983).

[12] A. M. Albano, J. Muench, C. Schwartz, A. I. Mees, and P. E. Rapp, Phys. Rev. A **38**, 3017 (1988).

[13] F. Kaspar and H. G. Schuster, Phys. Rev. A **36**, 842 (1987).

[14] J. Theiler, Phys. Rev. A **34**, 2427 (1986).

[15] C. Meneveau and K. R. Sreenivasan, Phys. Rev. Lett. **59**, 1424 (1987).

[16] J. Theiler, S. Eubank, A. Longtin, B. Galdrikian, and J. D. Farmer, Physica D **58**, 77 (1992).